NICKEL HYDROXIDE FILMS IN CONTACT WITH AN ELECTROACTIVE SOLUTION. A STUDY EMPLOYING ELECTROCHEMICAL IMPEDANCE MEASUREMENTS

RICARDO TUCCERI

Instituto de Investigaciones Fisicoquímicas Teóricas y Aplicadas (INIFTA), Conicet, Facultad de Ciencias Exactas (UNLP), Sucursal 4, Casilla de Correo 16, 1900, La Plata, Argentina

Abstract

The deactivation of nickel hydroxide films after prolonged storage times without use was studied. This study was carried out in the context of the Rotating Disc Electrode Voltammetry (RDEV) and Electrochemical Impedance Spectroscopy (EIS) when the nickel hydroxide film contacts an electroactive solution and a redox reaction occurs at the $Au\text{-}Ni(OH)_2$|electrolyte interface. Deferasirox (4-(3,5-bis(2-hydroxyphenyl)-1,2,4-triazol-1-yl) benzoic acid) was employed as redox species in solution. Limiting currents vs. electrode rotation rate dependences allowed one to obtain variation of the charge transport rate on the storage time. EIS was employed to obtain a more complete series of charge-transport parameters, that is, electron and ion diffusion coefficients and different interfacial resistances related to the gold/nickel hydroxide and nickel hydroxide/solution interfaces.

Keywords

Nickel hydroxide films; charge transport parameters; ion and electron diffusion coefficients; gold/nickel hydroxide and nickel hydroxide/solution interfacial resistances

1. INTRODUCTION

Nickel hydroxide is an important electroactive material that exhibits interesting electrochemical application [1-8]. Considering the important applications of nickel hydroxide electrodes, not many efforts have been made to study in detail their true durability and long-term stability. We have demonstrated in a previous work [9] that after storage without use for long time periods nickel hydroxide films deactivate, that is, the electron-transport rate is strongly reduced. The study reported in [9] was carried out in the context of the Rotating Disc Electrode Voltammetry (RDEV) for the interesting case where the nickel hydroxide-gold modified electrode contacts an electrolyte solution containing an electroactive substrate, such as, deferasirox (4-(3,5-bis(2-hydroxyphenyl)-1,2,4-triazol-1-yl) benzoic acid) [9-12]. The present study is a continuation of the previous one [9], where Electrochemical Impedance Spectroscopy (EIS) was employed to obtain the change of a more complete series of transport parameters of nickel hydroxide films with the storage time without use, that is, ion and electron diffusion coefficients and different interfacial resistances related to the gold/nickel hydroxide and nickel hydroxide/solution interfaces.

2. EXPERIMENTAL

The same electrodes and cell described in [9] were employed in this work. Electrode potentials are referred to the SCE in this work. Nickel hydroxide films employed here were also synthesized and stabilized as described in previous work [9]. These nickel hydroxide modified electrodes are called here, non deactivated (or immediately prepared). Fig. 1 shows a stabilized cyclic voltammogram at a scan rate 0.02 V s^{-1} in a 0.1 M NaOH solution for a non deactivated nickel hydroxide film whose voltametric charge value is 2 mC cm^{-2}. It was demonstrated in [9] that when these films are stored without use for long time periods, they undergo a deactivation process which is reflected in their conducting properties. These films were called in [9] deactivated films.
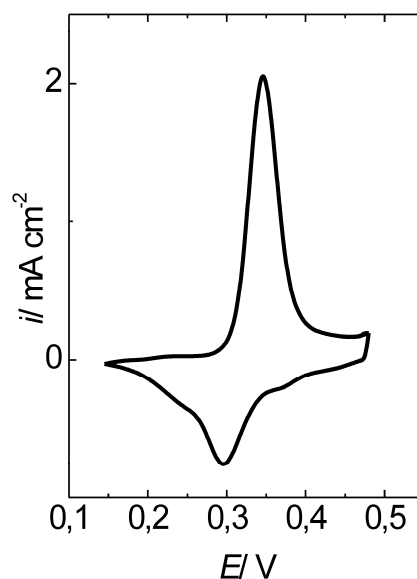
Figure 1. Cyclic voltammogram of a nondeactivated Au/Ni-hydroxide modified electrode.

Electrolyte: 0.1 M NaOH. Scan rate: 0.02 V s^{-1}. Voltammetric charge value of the nickel hydroxide film: Q = 2 mC cm^{-2}.

As in [9], steady-state experiments were performed here with both nondeativated and deactivated nickel hydroxide gold-modified electrodes in contact with a 0.1 M NaOH + 2 x 10^{-3} M deferasirox solution. Current-potential (*I-E*) curves were recorded at different electrode rotation rates (*Ω*). The electrode rotation rate Ω was controlled with home-made equipment that allowed one to select a constant Ω value in the range 50 rev min^{-1} < Ω < 8000 rev min^{-1}. This electrode rotation rate was controlled with a digital phototachometer (Power Instruments model 891). Impedance diagrams were recorded within the potential region comprised between 0.35 V to 0.5 V employing a PAR 309 system.

AR grade chemicals were employed throughout. Ni(NO$_3$)$_2$ Fluka was employed. NaOH (Merck) was used without purification. The solutions were prepared with water purified as described in [11].

3. RESULTS AND DISCUSSION

3.1. RDEV measurements

Six nickel hydroxide films all of the same charge value (Q = 2 mC cm^{-2}) were prepared. Each one of the 6 nickel hydroxide films, after being equilibrated within the potential region 0.0 V < E < 0.6 V in the 0.1 M NaOH solution (Fig. 1), was stored in the same solution for different times periods (Table 1). As described in [9] steady-state current potential curves were also recorded in this work for both nondeactivated and deactivated nickel hydroxide films in the presence of deferasirox (not shown). Anodic diffusion-limited currents ($I_{Lim,a}$) are observed at $E > 0.45$ V (*vs.* SCE). Fig. 2 compares anodic limiting current vs. Electrode rotation rate ($I_{Lim,a}$ vs. $\Omega^{1/2}$) dependences for nondeactivated and deactivated films. As can be seen from Fig. 2, the anodic limiting current for the nondeactivated film follows the Levich equation (linear $I_{Lim,a}$ vs. $\Omega^{1/2}$ dependence). The behaviour is associated to a rapid electron-transfer mediation at the nickel hydroxide/deferasirox solution interface. As can be seen from Fig. 2, after a given Ω value, the anodic limiting current for a deactivated film becomes independent of the electrode rotation rate. Also, as the more deactivated is the film, the lower is the electrode rotation rate at which a constant current value is reached. The constant currents are indicative of a deactivation process [9]. In Table 1 are listed the constant current values I_{const} achieved for the different storage times at which the nickel hydroxide film of 2 mC cm^{-2} was subjected.
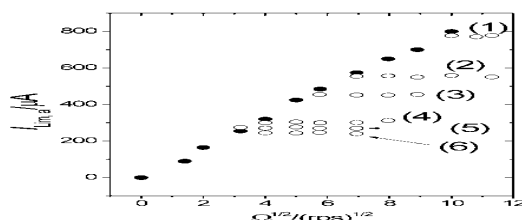
Figure 2. Levich representations ($I_{lim,a}$ *vs.* $\Omega^{1/2}$) for a nondeactivted (●) and different deactivated nickel hydroxide films. Solution: 0.1 M Na(OH) + 2 x 10^{-3} M deferasirox. Numbers indicate different storage times: (1) 10 h; (2) 20 h; (3) 25 h; (4) 45 h; (5) 65 ; (6) 85 h. Q = 2 mC cm^{-2} (Γ = 2.96 x 10^{-8} moles cm^{-2}).

[a] t/h	[b] $10^6 I_{const}/\mu A$ Q = 2 mC cm^{-2}	[c] $10^7 D_{ct}/cm^2$ s^{-1}
10	775	2.14
20	550	1.52
25	455	1.26
45	320	0.88
60	290	0.80
80	270	0.75

Table 1. I_{const} values for deactivated nickel hydroxide films of different thickness.

Electrode area: 0.7 cm^2. [a]Storage time. [b]I_{const} constant current for the different deactivated films. Q is the voltammetric charge value for the different deactivated films [c]D_{ct} diffusion coefficient values extracted form Eq. (1).

The constant current I_{const} was interpreted in [9] employing Eq. (1): [13]:

$$I_{const} = n\,F\,A\,D_{ct}\,(c_o/\phi_{film}) \qquad (1)$$

The charge transport process in different electroactive materials has been previously descried employing Eq. (1), where c_o is the total volumetric concentration of redox sites into the electroactive film and ϕ_{film} the film thickness. D_{ct} represents a measure of the charge transport rate within the film. Then, the charge diffusion process across nickel hydroxide-gold modified electrodes is here described in terms of Eq. (1). The parameter n represents the number of exchanged electrons between Ni(II)/Ni(III) sites. A and F are the electrode surface area and the Faraday´s constant, respectively. The limiting current value at which $I_{Lim,a}$ (= I_{const}) becomes constant was considered in [9] as a representation of the maximum flux of charge transported across the electroactive film.

Considering a uniform and homogeneous film ($\phi_{film} = \Gamma/c_o$), Eq. (1) can be written as:

$$I_{const} = n\,F\,A\,D_{ct}\,(c_o^2/\Gamma) \qquad (2)$$

Considering that c_o remains constant, the deactivation of nickel hydroxide films was attributed in [9] to a reduction of the charge propagation rate, D_{ct} (see third column in Table 1). The existence of a constant current I_{const} in a deactivated electroactive film was explained in [9]. In this regard, the I_{const} decrease with the storage time was here attributed to a D_{ct} decrease. In this connection, the electron diffusion coefficient, D_{ct}, has been expressed in terms of the mean distance between adjacent active redox sites (a) according to $D_{ct} = (a^2 k_o)$ [20], where the constant k_o shows an exponential decrease with the a increase [20]. Thus, the D_{ct} decrease could explain the electron current I_{const} decrease with the increase of the storage time [9].

3.2 Impedance measurements

Impedance measurements were also performed in the present work with nondeactivated and deactivated nickel hydroxide gold-modified electrodes of $Q = 2$ mC cm^{-2} contacting a 0.1 M Na(OH) + 2 x 10^{-3} M deferasirox solution at potential values $E > 0.35$ V. Nyquist diagrams at different electrode rotation rates for a nondeactivated nickel hydroxide film are shown in Fig. 3.
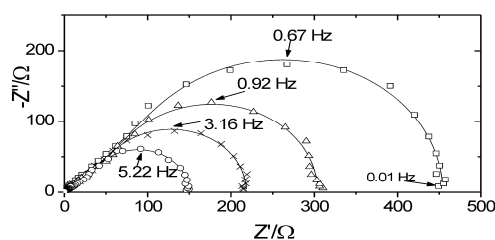
Figure 3. *Ac* impedance diagrams in the Nyquist coordinates (*-Z'' versus Z*) obtained at *E* = 0.5 V for a nondeactivated nickel hydroxide film. The different diagrams correspond to

differentelectrode rotation rates, Ω : ( ) 100 rpm; (Δ) 200 rpm; (X) 300 rpm; (O) 600 rpm. Electrolyte:0.1 M Na(OH) + 2 x 10^{-3} M deferasirox solution. $Q = 2$ mC cm^{-2}. Discrete points are experimental data and continuous lines represent the fitting by using the theory given in [21].

Impedance diagrams of each one of the six deactivated nickel hydroxide films indicated in Table 1 exhibit two loops (Fig. 4). While the loop at low frequency is Ω dependent, the high-frequency semicircle is independent of this variable. However, the size of the high-frequency semicircle depends on the storage time (Fig. 5). In this regard, at a given Ω value, the higher the storage time value is, the greater the high-frequency semicircle becomes.
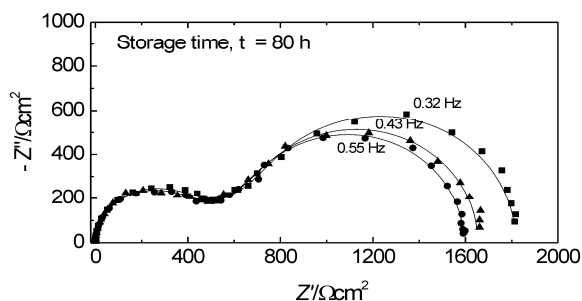
Fig. 4. *Ac* Impedance diagrams in the Nyquist coordinates (-*Z*" *versus Z*) obtained at *E* = 0.5 V for a deactivated nickel hydroxide film, storage time, 80 h.

The different diagrams correspond to different electrode rotation rates, Ω : (■) 1000 rpm ; (▲) 1500 rpm; (●) 3000 rpm. Electrolyte: 0.1 M Na(OH) + 2 x 10^{-3} M deferasirox solution. $Q = 2$ mC cm^{-2}. Discrete points are experimental data and continuous lines represent the fitting by using the theory given in [21].

Although several *ac* impedance diagrams at potential values within the range 0.35 V < *E* < 0.5 V (*versus* SCE) were recorded for different deactivated nickel hydroxide films, those shown in Figs. 3 to 5 were considered as representative of the potential region where the redox reaction at the nickel hydroxide/deferasirox solution occurs.
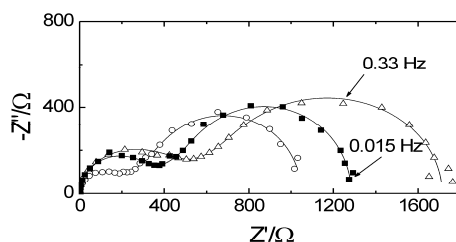
Fig. 5. *Ac* Impedance diagrams in the Nyquist coordinates (-*Z*" *versus Z*) obtained at *E* = -0.2 V and a constant electrode rotation rate, Ω = 3000 rpm, for three deactivated nickel hydroxide films: (O) *t* = 25 h; (■) *t* = 45 h; (Δ) *t* = 80 h. Electrolyte: 0.1 M Na(OH) + 2 x 10^{-3} M deferasirox solution. $Q = 2$ mC cm^{-2}. Discrete points are experimental data and continuous lines represent the fitting by using the theory given in [21].

3.3 Interpretation of impedance spectra

The general theory of *ac* impedance described by Vorotyntsev et al. in [21] was employed to interpret experimental impedance data of the gold-nickel hydroxide film/electrolyte system. It should be indicated that the theory developed in [21] is strictly valid when the charging of interfacial double layers is negligible, i.e., it does not account for the charging of the film|substrate and film|solution layers in parallel with the processes of injection of charge carriers. If this is not the case, a more complete model, such as the one developed by Vorotyntsev in [22], should have to be used. In this model [22], besides the traditional "double-layer" capacitance and interfacial charge-transfer resistances, two additional parameters for each boundary, "interfacial numbers" for each species and "asymmetry factors," are introduced. Although we also fitted our experimental impedance diagrams with the model reported in [22], the fitting did not result much more precise than that using the model given in [21], and furthermore, the increasing mathematical difficulty of determining the numerous parameters of the model given in [22] from experimental data was a major drawback. Then, despite this last theoretical limitation, the model described in [21] concerning a uniform and nonporous film and no penetration of redox species from the solution was employed to interpret our experimental impedance diagrams.

As in the present case one has the modified electrode geometry with a redox active electrolyte solution (m|film|es), Eq. (41) of Ref. [21] (Eq. (3) in this work) must be applied

$$Z_{m|film|es} = R_{m|f} + R_f + R_s + [Z_e^{f|s} R_i^{f|s} + W_f Z_{12}^m] (Z_e^{f|s} + R_i^{f|s} + 2 W_f \coth 2\nu)^{-1} \tag{3}$$

where

$$Z_{12}^m = Z_e^{f|s} [\coth \nu + (t_e - t_i)^2 \tanh \nu] + R_i^{f|s} 4t_i^2 \tanh \nu + W_f 4t_i^2 \tag{4}$$

In Eqs. (3) and (4):

$\nu = [(j\omega\phi_p^2)/4D]^{1/2}$ is a dimensionless function of the frequency ω, ϕ_p is the film thickness, D is the binary electron-ion diffusion coefficient, and t_i and t_e are the migration (high frequency) bulk-film transference numbers for anions and electrons, respectively. D and $t_{i,e}$ depend on the electron and ion diffusion rates (D_e and D_i). $W_f = [\nu/j\omega\phi_p C_p] = \Delta R_f/\nu$ is a Warburg impedance for the electron-ion transport inside the electroactive film. ΔR_f $(=\phi_p/4DC_p)$ is the amplitude of the Warburg impedance inside the film, and C_p is the redox capacitance per unit volume.

R_f $(=\phi_p/\kappa)$ is the high-frequency bulk-film resistance, R_s the ohmic resistance of the bulk solution (κ is the high-frequency bulk conductivity of the film), $R_{m|f}$ is the metal|film interfacial electron-transfer resistance, and $R_i^{f|s}$ is the film|solution interfacial ion-transfer resistance.

$Z_e^{f|s} = (R_e^{f|s}+W_s)$ is the electronic impedance, where $R_e^{f|s}$ is the interfacial electron-transfer resistance at the film|solution interface, and W_s is the convective diffusion impedance of redox species in solution, which contains the bulk concentrations of ox(red) forms, $c_{ox}(c_{red})$, and their diffusion coefficients inside the solution, $D_{ox}(D_{red})$. Also, it contains the Nernst layer thickness, δ. The electron-transfer resistance at the nickel hydroxide film/solution interface is defined in terms of the redox cuple concentration in solution [21].

Diffusion of the redox forms from the bulk solution to the film|solution interface can be regarded as stationary through the diffusion layer thickness, expressed in cm by

$$\delta = 4.98 D_{ox,red}^{1/3} \eta^{1/6} \Omega^{-1/2} \tag{5}$$

where η is the kinematic viscosity of the solution in the same units as $D_{ox,red}$, and Ω the rotation rate of the disk electrode in rpm. The rest of the constants have their usual meaning. This model also includes the impedance behavior of the electoactive material contacting the inactive electrolyte (absence of the redox couple in solution) by considering $Z_e^{f|s} \to \infty$ in Eq. (3).

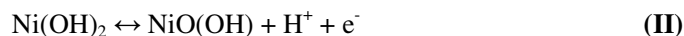## 3.4 Dependence of the different charge-transport parameters on the storage time

Continuous lines on the impedance diagrams shown from Figs. 3 to 5 are simulated curves calculated by using Eq. (3).

A good fitting was observed for the different impedance diagrams. The fitting procedure by using Eq. (3) was based on the CNLS (Complex Nonlinear Squares) method. A rigorous fitting procedure was performed according to the method described in previous works [23-26].

In the simulations the number of transferred electrons, n, was assumed to be 1. In this regard, the redox system corresponding to the peaks shown in Fig. 1 can be represented by the following electrochemical reaction [27]

$$Ni(OH)_2 + HO^- \leftrightarrow NiO(OH) + H_2O + e^- \qquad \textbf{(I)}$$
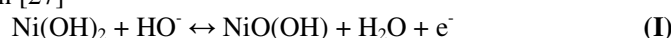
or as done in [28,29], by:

$$Ni(OH)_2 \leftrightarrow NiO(OH) + H^+ + e^- \qquad \textbf{(II)}$$

The oxidation of deferasirox on the nickel hydroxide film surface can be represented as:

$$Ni(II) \to Ni(III) + 1e^- \qquad \textbf{(III)}$$

$$Ni(III) + drug \to Product + Ni(II) \qquad \textbf{(IV)}$$
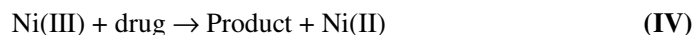
Diffusion coefficient values around 10^{-5} cm^2 s^{-1} were considered for deferasirox in solution. The bulk concentrations of the redox substrate species were considered equal ($c_{ox} = c_{red} = 2 \times 10^{-6}$ mol cm^{-3}). The nickel hydroxide film thickness was calculated on the basis of the expression $\phi_{film} = \Gamma/c_o$. By considering a charge value of $Q = 2$ mC cm^{-2}, a nickel hydroxide film thickness about 27 nm results. The value of the total redox site concentration obtained from RDEV measurements (3.86×10^{-3} mol cm^{-3} [9]) was employed to fit experimental impedance plots. The ohmic resistance of the solution in contact with the nickel hydroxide films, R_S, was measured. A value $R_S \sim 2.19$ ohm cm^2 was obtained. Then, by considering the high-frequency intercept of impedance diagrams of nickel hydroxide films in the presence and in the absence of deferasirox as R_o, the high-frequency bulk nickel hydroxide film resistance, R_f, was calculated as $R_f = R_o - R_S$ [30]. The latter value varied within the range $3.09 < R_f < 5.34$ ohm cm^2 and it seems not to be strongly dependent on the storage time. Then, R_f and R_S values were imposed in the fitting. The remnant parameters contained in Eq. (3) ($R_{m|f}$, $R_i^{f|s}$, $R_e^{f|s}$, C_p, D_e and D_i) were calculated from the experimental impedance data by the fitting procedure described above. The first four parameters (C_p, $R_{m|f}$, $R_i^{f|s}$ and $R_e^{f|s}$) were varied without restraints during the fitting. However, some reference values were considered for D_e and D_i. For the nondeactivated nickel hydroxide film thickness used in this work ($\phi_p = 27$ nm), D_e and D_i values were allowed to vary within the range 10^{-7}-10^{-11} cm^2 s^{-1}, in such a way that diffusion coefficient values lower than 10^{-11} were considered unrealistic for these thick films. That is, D_e and D_i values lower than 10^{-11} were only obtained from impedance diagrams (not shown) of very thin nickel hydroxide films ($Q_{T,Red} = 0.04$ mC cm^{-2}, $\phi_p = 3$ nm), where incomplete coating of the metal area by the thin nickel hydroxide film is possible. A contribution of the interfacial capacitance, C_H, also considered as a fitting parameter, was included in order to represent the actual impedance diagrams from the calculated ones.

Different charge-transport and charge-transfer parameters versus the storage time dependences, extracted from the fitting procedure described above, are shown from Figs. 6 to 11.

The C_p *versus* storage time dependence is shown in Fig. 6. Starting from a C_p value of about 87 F cm^{-3}, for a nondeactivated film, a decrease of C_p with increasing the storage time is observed. It should be kept in mind that these C_p values correspond to the oxidized state of the nickel hydroxide film.
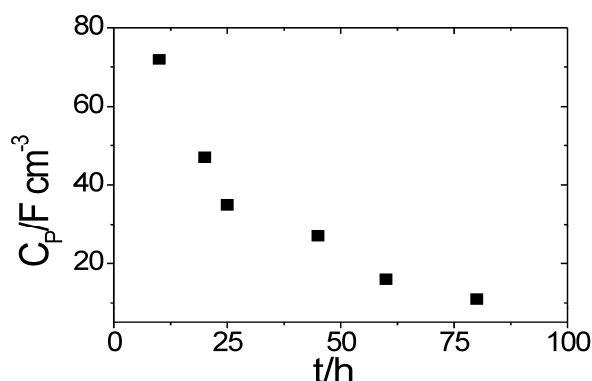

Figure 6. Redox capacitance (C_p) vs. storage time dependence. The value 87 F cm^{-3} for $t = 0$ corresponds to a nondeactivated nicel hydroxide film. Electrolyte: 0.1 M Na(OH) + 2 x 10^{-3} M deferasirox solution.
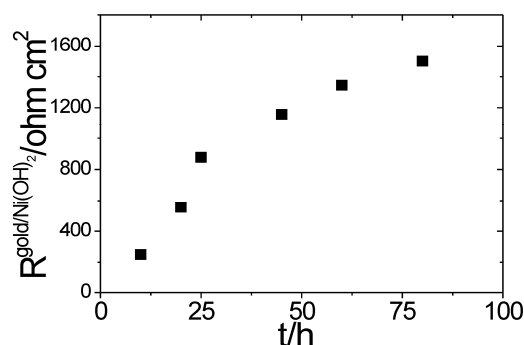
$$Q = 2 \text{ mC cm}^{-2}.$$

Nickel hydroxide film-solution interfacial ion-transfer resistance ($R_{ion}^{Ni(OH)_2/elect}$) and Gold/Ni(OH)$_2$ interfacial electron-transfer resistance ($R^{gold/Ni(OH)2}$) on storage time dependences are shown in Figs. 7 and 8, respectively. $R_{ion}^{Ni(OH)_2/elect}$ as a function of the storage time exhibits a different feature as compared with $R^{gold/Ni(OH)2}$. That is, while $R^{gold/Ni(OH)2}$ seems to Increase continuously within the whole storage time range, $R_{ion}^{Ni(OH)_2/elect}$ firstly exhibits a slight increase within the range $0 < t < 25$ h and then, a strong increase is observed within the range 25 h $< t < 80$ h. Also, the magnitude of $R_{ion}^{Ni(OH)_2/elect}$ and $R^{gold/Ni(OH)2}$ change within the whole storage time range is different. $R_{ion}^{Ni(OH)_2/elect}$ change is around one order of magnitude lower than $R^{gold/Ni(OH)2}$ change. This difference could indicate that the high-frequency semicircle on impedance diagrams (Figs. 3 to 5) is mainly determined by $R^{gold/Ni(OH)2}$. The increase of interfacial $R^{gold/Ni(OH)2}$ resistance could be due to an increasing number of inactive sites at the Gold|Ni(OH)$_2$ interface with the increase of deactivation.

Nickel hydroxide/electrolyte interfacial electron-transfer resistance ($R_{electron}^{Ni(OH)2|elect}$) values were also extracted from the fitting procedure. The feature of $R_{electron}^{Ni(OH)2|elect}$ *versus* storage time dependence (Fig. 9) is similar to $R^{gold/Ni(OH)2}$ *versus* storage time dependence (Fig. 8). However, the $R_{electron}^{Ni(OH)2|elect}$ values are around 20 times lower than $R^{gold/Ni(OH)2}$ values. Also, it is interesting to note that the $R_{electron}^{Ni(OH)2|elect}$ change is lower than the $R_{ion}^{Ni(OH)_2/elect}$ change, particularly at high storage times. The increase of interfacial $R_{electron}^{Ni(OH)2|elect}$ resistance could be due to an increasing number of inactive sites at the Ni(OH)$_2$|solution interface with the increase of deactivation.
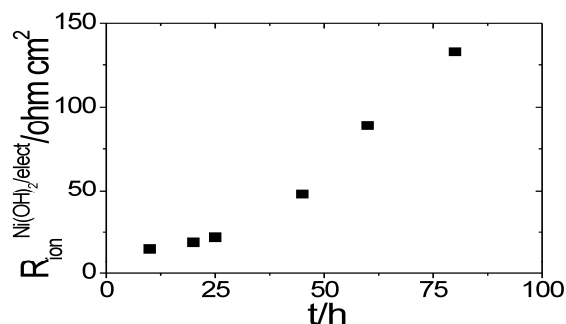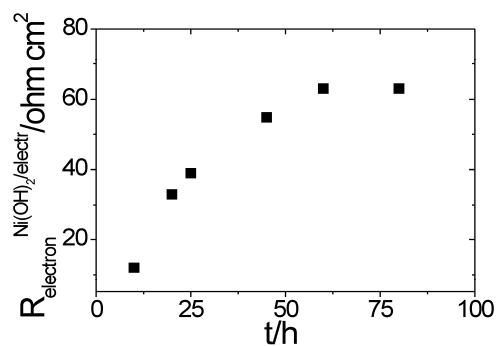
Figure 7. Nickel hydroxide film-solution interfacial ion-transfer resistance as a function of the storage time. Electrolyte: 0.1 M Na(OH) + 2 x 10^{-3} M deferasirox solution. $Q = 2$ mC cm^{-2}.

Figure 8. Gold/Ni(OH)$_2$ interfacial electron-transfer resistance ($R^{Gold/Ni(OH)2}$) as a function of the storage time. Electrolyte: 0.1 M Na(OH) + 2 x 10^{-3} M deferasirox solution. $Q = 2$ mC cm^{-2}.


Figure 9. Interfacial electron-transfer resistance ($R_{electron}^{Ni(OH)2|elect}$) as a function of the storage time. Electrolyte: 0.1 M Na(OH) + 2 x 10^{-3} M deferasirox solution. $Q = 2$ mC cm^{-2}.
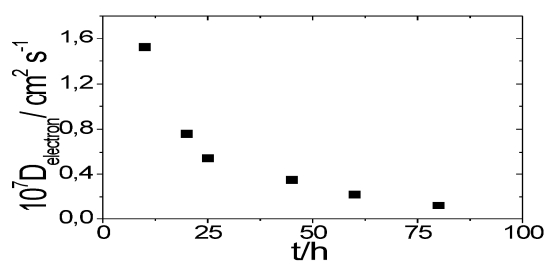
Ion and electron diffusion coefficients *versus* storage time dependences are shown in Figs. 10 and 11, respectively. Both diffusion coefficients decrease with the storage time increase. As was proposed from RDEV data, the decrease of $D_{electron}$ with the increase of the storage time could be attributed to an increase of the hopping distance between remnant redox active sites after nickel hydroxide deactivation. $D_{electron}$ values are nearly one order of magnitude higher than D_{ion} values. In the present work, relative diffusion coefficient values ($D_{electron} > D_{ion}$) refer to the oxidized state

of nickel hydroxide films. Another interesting difference between $D_{electron}$ and D_{ion} *versus* the storage time dependences can be observed by comparing Fig. 10 with Fig. 11. While D_{ion} remains nearly constant for low storage times (0 < t < 25 h), $D_{electron}$ decreases continuous and rapidly within this storage time range. This finding seems to indicate that although ion motion always controls the charge-transport process at nickel hydroxide films, the influence of the electron motion on the whole charge-transport process becomes more pronounced at a high storage times. Then, a break seems to be observed at around 25 h, in the D_{ion} *versus* the storage time dependence. The break also becomes evident in nickel hydroxide film-solution interfacial ion-transfer resistance as a function of the storage time. (Fig. 7). It is possible that both parameters $R_{ion}^{Ni(OH)_2/elect}$ and D_{ion} are related to proton movements across the nickel hydroxide film|solution interface and inside the nickel hydroxide film, respectively. Diffusion of protons [31] has been considered to control both charge and discharge processes in many rechargeable battery systems [31]. A great discrepancy is observed between the proton diffusion coefficient values reported by the different researchers. It is found that diffusion coefficient of protons decreases from 3.4×10^{-8} $cm^2\ s^{-1}$ to $3.7 \times 10^{-9}\ cm^2\ s^{-1}$ as the electrode changes from fully charged to 30% state of charge. The value of the diffusion coefficient further decreases by another one and a half order of magnitude to $6.4 \times 10^{-11}\ cm^{2}\ s^{-1}$ at the completely discharged state. Then, our values of D_{ion} around $10^{-8}\ cm^2\ s^{-1}$ (Fig. 10) for the oxidized state of the nickel hydroxide film seems to be in coincidence with proton diffusion coefficient values reported for other researchers [31].

With regard to C_H values, starting from a value of around 25 $\mu F\ cm^{-2}$ for a nondeactivated nickel hydroxide film, C_H decreases in a nearly continuous way as the storage time increases, reaching a value of about 10.4 $\mu F\ cm^{-2}$ for t = 80 h (not shown). The C_H decrease is similar to the $R^{Gold/Ni(OH)2}$ increase (Fig. 8). Again, this effect could be assigned to the creation of inactive gaps in the redox site configuration at the nickel hydroxide film |gold interface with deactivation.
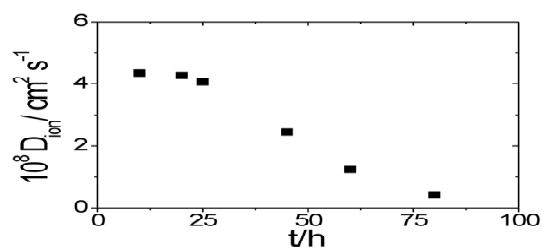
Figure 10. Ion diffusion coefficient (D_{ion}) as a function of the storage time. Electrolyte: 0.1 M Na(OH) + 2 $\times 10^{-3}$ M deferasirox solution. $Q = 2$ mC cm^{-2}.

Fig. 11. Electron diffusion coefficient ($D_{electron}$) as a function of the storage time. Electrolyte: 0.1 M Na(OH) + 2 x 10^{-3} M deferasirox solution. $Q = 2$ mC cm^{-2}.

4. CONCLUSIONS

Nickel hydroxide films are deactivated under storage time without use. The reduction of the conductivity of nickel hydroxide films was demonstrated employing Rotating Disc Electrode Voltammetry and Impedance measurements in the presence of deferasirox. While the first technique allows one to obtain an electron diffusion coefficient value the second one allows one obtaining electron and ion diffusion coefficient values and different interfacial charge-transfer resistances. Ion diffusion coefficient values seem to be in agreement with proton diffusion coefficient values reported for nickel hydroxide in the field of rechargeable batteries. While both ion and electron diffusion coefficient values decrease with the deactivation of nickel hydroxide films, the different interfacial resistances increase as the storage time of the nickel hydroxide film increases. The results of this work demonstrate the limited durability of the nickel hydroxide films electrochemically synthesized under storage for prolonged time periods.

REFERENCES

[1] Berchmans, S.; Gomathi, H.; Rao, G.P., (1995) Electrooxidation of alcohols and sugars catalysed on a nickel oxide modified glassy carbon electrode, J. Electroanal. Chem. Vol. 394, pp. 267-270.

[2] Lo, Y.L.; Hwang, B.J., (1995) Kinetics of ethanol oxidation on electroless NiP/SnO2/Ti in KOH solutions, J. Electrochem. Soc. Vol. 142, pp. 445-450.

[3 Madji, S.; Jabbari, A.; Heli, H., (2007) A study of the electrocatalytic oxidation of aspirin on a nickel hydroxide-modified nickel electrode, J. Solid State Electrochem. Vol. 11, pp. 601-607.

[4] Gobi, K.V.; Tokuda, K.; Ohsaka, T. (1998), Monomolecular films of a Ni(II) pentaazamacrocyclic comples for the electrocatalytic oxidation of hydrogen peroxide at gold electrodes J. Electroanal. Chem. Vol. 444, pp. 145-150.

[5] Jafarian, M.; Mahjani, M.G.; Heli, H. (2003); Gobal, F.; Heydarpoor, M., Electrocatalytic oxidation of methane at nickel hydroxide modified nickel electrode in alkaline solution Electrochem. Commun. Vol. 5, pp. 184-188.

[6] Madji, S.; Jabbari, A.; Heli, H.; Moosavi-Movahed, A.A. (2007), Electrocatalytic oxidation of some amino acids on a nickel-curcumin complex modified glassy carbon electrode Electrochim. Acta Vol. 52, pp. 4622-4629.

[7] Shibli, S.M.A., Beenakumari, K.S.; Suma, N.D. (2006), Nano nickel oxide/nickel incorporated nickel composite coating for sensing and estimation of acetylcholine. Biosens. Bioelectron. Vol. 22, pp. 633-638.

[8] Yi, S.Y.; Chang, H.Y.; Chao, H.; Park, Y.C.; Lee, S.H.; Bae, Z.U. (2007), Resolution of dopamine and ascorbic acid using Ni(II) complex polymer-modified electrodes J. Electroanal. Chem. Vol. 602, pp. 217-225.

[9] Kontoghiorghes, G.J.; Pattichis, K.; Neocleous, K.; Kolnagou, A. (2004), The design and development of deferiprone (L1) and others ion chelators for clinical use: targeting methods and application prospects Curr. Med. Chem. Vol. 11, pp. 2161-2183.

[10] Kontoghiorghes, G.J. (2001), Clinical use, therapeutic aspects and future potential of deferiprone in thalassemia and other conditions of iron and other metal toxicit, Drugs Today, Vol. 37, pp. 23-35.

[11] Hajjizadeh, M.; Jabbari, A.; Heli, H.; Mosavi-Movahedi, A.A.; Shaffiee, A.; Karimian, K. (2008), Electrocatalytic oxidation and determination of deferasirox and deferiprone on a nickel oxyhydroxide-modified electrode, Analytical Biochemistry, Vol. 373, pp. 337-348.

[12] Vilche, J.R.; Arvía, A.J. (1978), kinetics and mechanism of the nickel electrode. II Acid solutions containing high concentration of sulphate and nickel ions, Corros. Sci., Vol. 18, pp. 441-463.

[13] Seghiour, A.; Chevalet, J.; Barhoum, A.; Lantelme, F. (1998), Electrochemical oxidation of nickel in alkaline solutions: a voltammetric study and modeling, J. Electroanal. Chem., Vol. 442, pp. 113-123.

[14] Haring, P.; Kotz, R. (1995), Nanoscale thickness change of nickel hydroxide films during electrochemical oxidation reduction monitored by in situ atomic force microscopy, J. Electroanal. Chem., Vol. 385, pp. 273-277.

[15] Deslouis, C.; Tribollet, B. (1992), Advances in Electrochemical Science and Engineering, en: Gerischer, H.; Tobias, C. (Eds.), Vol. 2, pp. 205, VCH Publishers, New York, USA.

[16] Ybarra, G.; Moina, C.; Florit, M.I., Posadas, D. (2007), Redox mediation at electroactive coated polymer electrodes: Mechanistic diagnosis criteria from steady state polarization curves, J. of Electroanal. Chem., Vol. 609, pp. 129-139.

[17] Ybarra, G.; Moina, C.; Florit, M.I., Posadas, D. (2008), Current rectification by mediating electroactive polymers, Electrochim. Acta, Vol. 53, pp. 3955-3959.

[18] Bonfranceschi, A.; Pérez Córdoba, A.; Keunchkarian, S.; Zapata, S.; R. Tucceri, R. (1999), Transport across poly(o-aminophenol) modified electrodes in constact with media containing redox active couples. A. study using rotating disc electrode voltammetry, J. Electroanal. Chem. Vol. 477, pp. 1-13.

[19] Rodríguez Nieto, F.J.; Posadas, D.; Tucceri, R. (1997), Effect of the bathing electrolyte concentration on the charge transport process at poly(o-aminophenol) modified electrodes. An ac impedance study, J. Electroanal. Chem., Vol. 434, pp. 83-91.

[20] Tucceri, R. (2009), Redox mediation and permeation process at deactivated poly(o-aminophenol) films. A study applying rotating disc electrode voltammetry and electrochemical impedance spectroscopy, J. Electroanal. Chem., Vol. 633, pp. 198-206.

[21] Tucceri, R. (2011), Charge-transfer and charge transport parameters of deactivated poly(o-aminophenol) film electrodes. A study employing electrochemical impedance spectroscopy, J. Electroanal. Chem., Vol. 659, pp. 83-91.

[22] Bisquert, J. (2002), Analysis of the kinetics of ion intercalation: Ion trapping approach to solid-state relaxation processes, Electrochim. Acta, Vol. 47, pp. 2435-2449.

[23] Chidsey, C.E.D.; Murray, R.W. (1986), Redox capacity and direct current conductivity in electroactive polymers, J. Phys. Chem., Vol. 90, pp. 1479-1484.

[24] Zerbino, J.O.; de Pauli, C.; Posadas, D.; Arvía, A.J. (1992), Ellipsometry of nickel hydroxide electrodes formed by ex situ chemical precipitation. Potential routine and time effects, J. Electroanal. Chem., Vol. 330, pp. 675-691.